Int. J. Electrochem. Sci., 13 **(2018)** 1879 – 1892, doi: 10.20964/2018.02.17

International Journal of
ELECTROCHEMICAL
SCIENCE
www.electrochemsci.org

The effects of Zn^{2+} and Polyacrylamide (PAM) on the Electrodeposition of Manganese from Non-Selenium Sulfate Solutions

Fan Zheng[1], *Yan Li*[1], *Dihua Wang*[1], *Jinlin Li*[2], *Hua Zhu*[1,*]

[1] School of Resources and Environmental Science, Wuhan University, Wuhan 430079, People's Republic of China
[2] College of Chemistry and Material Science, South-Central University for Nationalities, Wuhan 430074, People's Republic of China
[*]E-mail: zhuhua@whu.edu.cn

Received: 2 October 2017 / *Accepted:* 23 November 2017 / *Published:* 28 December 2017

In the present paper, the additives of Zn^{2+} and polyacrylamide (PAM) were used to increase the cathodic current efficiency and improve the morphology of deposits. The effects of Zn^{2+} and polyacrylamide (PAM) on the electrodeposition of manganese from non-selenium solutions were investigated by cyclic voltammetry. The morphology and structure of the deposited metal obtained by galvanostatic electrolysis was determined by scanning electron microscope (SEM) and X-ray diffraction (XRD), and the purity was determined by X-ray fluorescence (XRF) spectrometry. The results indicated that Zn^{2+} could increase the current efficiency by 2% when 2 $mg \cdot L^{-1}$ Zn^{2+} was added, but it could not improve the morphology of the deposited metal. On the contrary, the incorporation of PAM slightly decreased the current efficiency, but it was demonstrated dramatic leveling and refining effects on the morphology of the cathodic deposits by promoting nuclei formation. The combination of Zn^{2+} and PAM exerted a beneficial effect on manganese deposition for long-term electrolysis, meanwhile, the manganese purity could reach up to 99.90%.

Keywords: Additive; Electrodeposition; Manganese; Current efficiency; Deposit Morphology

1. INTRODUCTION

Manganese is a vital metal in industry and used in many products, particularly in the steelmaking industry, which is accounted for 90% of the metallic manganese consumption worldwide [1].

It is well known that metallic manganese (Mn) is obtained from manganese sulfate media at commercial practice. However, it should be mentioned that the electrodeposition of manganese is

difficult because of the very negative reduction potential of Mn^{2+} (E^0 = -1.18 V vs. SCE), which results in a low current efficiency. Therefore, many researchers have attempted to increase the cathodic efficiency by introducing additives such as selenium and tellurium compounds [2-7]. Recently, Fan [8] characterized the Mn-Se interaction at the cathode interface during the electrolytic process, and found the formation of α-MnSe plays a critical role in cathodic efficiency. Jiao [9] and Sun [10] reported that the addition of SeO_2 could inhibit the hydrogen evolution reaction and promote manganese electrodeposition. More specifically, the addition of SeO_2 increases the overpotential of manganese deposition in the low polarization region [11]. In addition, Griškonis [12] reported that the current efficiency increased from 37% to 71% when the bath temperature increases from 37°C to 71°C in the presence of 2.20 mmol·L^{-1} Te (VI) additive. However, the incorporation of selenium or tellurium compounds contaminates the deposited manganese with a concentration of 0.1% and 1.6 %, respectively [3, 12]. Moreover, they not only pollute the environment but also poses a health threat to the workers [13-14].

Hence, alternative additives have been sought in the industrial production of electrolytic manganese to counteract the detrimental effects of impurities. Sulfite compounds, such as SO_2, are promising additives, despite the current efficiency is only about 60% in industrial production [1, 15, 16]. Some researchers had tried to improve the current efficiency through purifying the electrolyte as the impurities in the electrolyte lower the hydrogen evolution overpotential [17]. Interestingly, Mantell and Ferment [18] produced pure manganese wherein a trace amount of zinc was added to the electrolyte. Lai [2] also reported that the current efficiency increased in the presence of a trace amount of zinc, which was usually considered as an impurity in the electrolytic process [11, 19, 20].

Another problem in the process of manganese electrodeposition is the dendritic growth that forms on the edge of the plate, which is detrimental in large-scale commercial practice when used for a long time. The coarse granular deposition on the cathode grows radially to form a cauliflower-like structure because of the uneven current distribution on the cathode. The metal tends to come off in individual nodules rather than sheets or plates and re-dissolves in the catholyte when the cathode is extracted from the cell. Moreover, the phenomenon of grain coarsening is more common in the non-selenium electrolyte media as higher Mn (II) concentration is used in this electrolyte to obtain higher current efficiency. Some researchers mentioned that the addition of polyacrylamide (PAM) can make the deposit compact and smooth [21-24].

Considering Zn^{2+} having a more positive reduction potential than Mn^{2+} in the sulfate electrolyte, which could be reduced prior to Mn^{2+} theoretically, the reduced Zn would be useful to promote the manganese deposition or reduce hydrogen evolution. In the meanwhile, PAM is regarded as an effective surfactant to inhibit the dendritic growth. Herein the objective of this study was to combine these two additives to get the optimal current efficiency and morphology during manganese electrodeposition. In addition, the preliminary mechanism of zinc and PAM in manganese electrodeposition was investigated by cyclic voltammetry, and the effect of the additives on product quality and current efficiency were investigated.

2. EXPERIMENTAL

2.1 Apparatus

The electrolytic cell was made of polymethyl methacrylate and divided into an anolyte chamber and a catholyte chamber by an anion exchange membrane, which was manufactured by JinQiu Environmental Water Treatment Co., Ltd and it could sufficiently prevent the acid permeating from the anodic compartment to the cathodic compartment [25]. The size of each chamber was 10.5 cm×10 cm×12.5 cm and the volume of electrolyte is 1 L. The cathodic deposition using a Neware galvanostat (Shenzhen, China) was carried out on a 316 L grade stainless steel cathode (4 cm × 2 cm) and a titanium-based Ir-Ta oxide coated anode and the cathodic current density was set at 50 $mA \cdot cm^{-2}$. The electrolytic cell was placed in a water bath at 40 °C ±2 °C.

2.2 Reagents

All reagents used, including manganese sulfate ($MnSO_4 \cdot H_2O$), ammonium sulfate ($(NH_4)_2SO_4$), ammonium sulfate ($(NH_4)_2SO_3 \cdot H_2O$, 91%), ammonium hydroxide ($NH_3 \cdot H_2O$), sulfuric acid (H_2SO_4), zinc sulfate ($ZnSO_4 \cdot 7H_2O$), potassium dichromate ($K_2Cr_2O_7$) and anionic polyacrylamide (PAM) (M_w=300,000) were analytic grade, purchased from Sinopharm Chemical Reagent Co., Ltd, China and used directly without further purification. Ultra-pure water with a resistivity of 18.25 MΩ · cm, obtained by using a water purification system (Wuhan, China), was used in all experiments. Analytical grade ammonia (1:1, v/v) was used to adjust the pH needed. The main additive SO_2 was in the form of $(NH_4)_2SO_3$. The working solution for electrodeposition contain 0.455 $mol \cdot L^{-1}$ $MnSO_4$ + 1.0 $mol \cdot L^{-1}$ $(NH_4)_2SO_4$ + 0.2 $g \cdot L^{-1}$ SO_2, pH 7.4, which represented as S_0.

2.3 Electrochemical experiments

A CHI potentiostat [ChenHua, Shanghai, China] was used for cyclic voltammetry experiments. The working electrode was a 316 L grade stainless steel with an active area of 0.78 cm^2. Saturated calomel electrode (SCE) and platinum foil served as a reference electrode and counter electrode, respectively. Electrochemical experiments were performed on a CHI660D electrochemical workstation (Shanghai Chenhua Instrument Co. Ltd., China) at a potential scan rate of 5 $mV \cdot s^{-1}$ in water bath at 40 °C ±2 °C.

2.4 Data processing

The cathode was passivated for 30s in 5 wt% potassium dichromate to prevent darkening of the deposit surface after each electrolysis experiment [26], and then washed with distilled water and dried in an oven.

The current efficiency was calculated using the following Eq.

$$\eta_c = \frac{M_c \times 1000}{E_{Mn} \times t \times I} \times 100\%$$

Where, η_c is the cathode current efficiency, M_c is the weight of the cathodal product (g), E_{Mn} is the electrochemical equivalent of Mn (g/A·h), t is the electrolytic time (h), and I is the applied current (A) in the experiments.

2.5 Characterization

The deposits were characterized using optical camera, metallographic microscope, scanning electron microscopy (SEM), X-ray diffractometry (XRD) and X-ray fluorescence (XRF) spectroscopy.

The external appearances of the deposits were evaluated using optical camera [Canon G12, Japan]. Particle size and micro-morphology were analyzed using a field-emission scanning electron microscopy [Zeiss Sigma FESEM, FEI Sirion fielf emission, Germany]. X'Pert Pro-XRD [PANalytical, Netherlands] with X-ray 6000 with Cu Kα1 radiation at λ=1.5405 Å was employed to study the crystal structure. Compositions of the deposits were determined by XRF using a S4 Pioneer model [Bruker AXS, Microanalysis GmbH, Berlin, Germany].

3. RESULT AND DISCUSSION

3.1. Polarization behaviors of Zn^{2+} and PAM on manganese electrodeposition

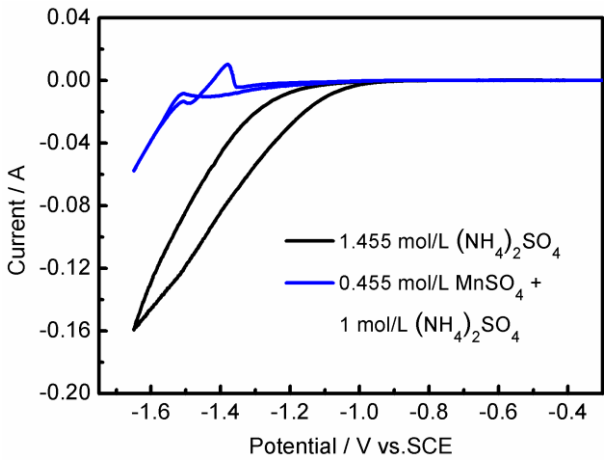

Figure 1. Cyclic voltammogram obtained on a 316 L stainless steel electrode in 0.455 mol·L^{-1} $MnSO_4$ + 1.0 mol·L^{-1} $(NH_4)_2SO_4$ and 1.455 mol·L^{-1} $(NH_4)_2SO_4$ from -1.65 V to -0.3 V at a scan rate of 5 mV·s^{-1}, concentration of SO_2 was 0.2 g·L^{-1}, pH 7.4 .

It was considered important to recognize the characteristics of hydrogen evolution reaction during the manganese deposition on the stainless steel cathode. Hence, the CV measurements in the solution with and without Mn (II) were firstly carried out respectively. The chosen solution with Mn (II) was 0.455 mol·L^{-1} $MnSO_4$ + 1.0 mol·L^{-1} $(NH_4)_2SO_4$, while the solution without Mn (II) was

designed as 1.455 M $(NH_4)_2SO_4$ to keep the same ion concentration and other parameters were stayed the same. The CV curves were shown in Fig. 1, in electrolyte without Mn (II), the main reducing process was hydrogen evolution reaction. It can be seen the hydrogen evolution onset potential was about -1.0 V, and then the reducing current increased continuously until the scanning potential ending to -1.65 V. On the backward scan, the current value lowered comparing to the forward scan, which should be attributed to the hydrogen bubble that adhered to the surface of electrode. While the electrolyte with Mn (II), manganese reduction and hydrogen evolution occured simultaneously during the cathodic polarization scan. Although the onset potential was almost similar, the rate of current increase was obviously reduced, which indicated that hydrogen evolution was inhibited by the preceding reduction step of manganese or trace amount manganese deposition [27]. Thereafter, with the scan potential moved negatively, the gradually increasing reduction step of manganese and hydrogen evolution was competed each other to form a current peak at -1.45 V. As the scan potential moved negatively to -1.52 V, the reduction current started to increase rapidly, which are owing to the substantial reduction of Mn (II). On switching the potential scan to the anodic direction from -1.65 V, the absolute value of the current was greater than that observed in the cathodic direction, which confirmed that Mn still deposited in this potential range. The anodic peaks located at about -1.38 V vs. SCE can be attributed to the oxidation of Mn. The higher anodic peak indicated that more Mn was deposited in the cathodic reduction reaction. Moreover, the integration of the charges associated with the oxidation and reduction reactions during the voltammogram, showed that the ratio, Qa / Qc (often called the stripping efficiency), was about 0.040. This also indicated that co-evolution of hydrogen was certainly a major contributor to the lack of charge balance.

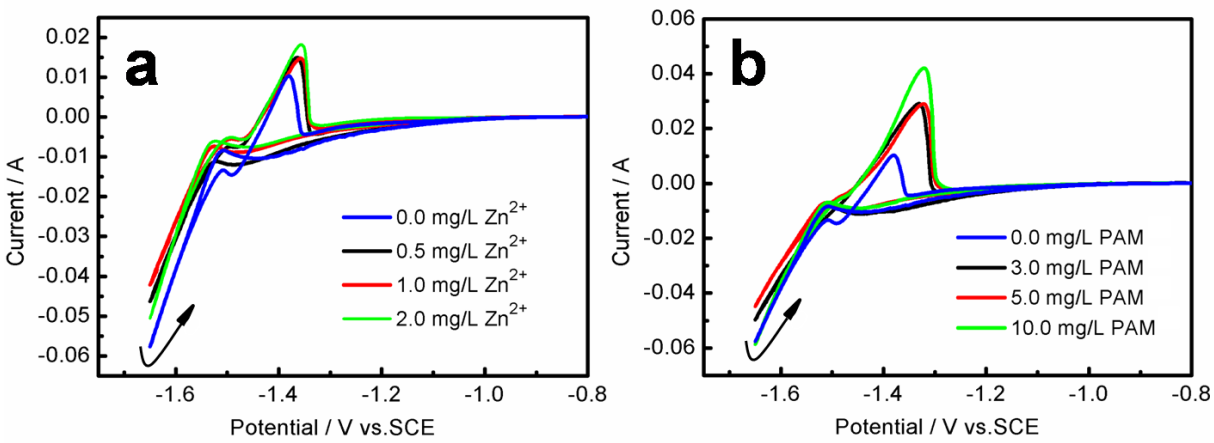

Figure 2. The cyclic voltammograms obtained on a 316 L stainless steel electrode in working solution 0.455 mol·L^{-1} $MnSO_4$ + 1.0 mol·L^{-1} $(NH_4)_2SO_4$ from -1.65 V to -0.8 V at a scan rate of 5 mV·s^{-1}. (a) C_{Zn2+} = 0.0, 0.5, 1.0, 2.0 mg·L^{-1}, (b) C_{PAM} = 0.0, 3.0, 5.0, 10.0 mg·L^{-1}, concentration of SO_2 was 0.2 g·L^{-1}, pH 7.4 .

Thus, since the current peak at -1.45 V should be attributed to hydrogen evolution, the effects of inhibition of hydrogen evolution can be identified from this current peak, cyclic voltammetrys were carried out in working electrolytes 0.455 mol·L^{-1} $MnSO_4$ + 1.0 mol·L^{-1} $(NH_4)_2SO_4$ and 0.455 mol·L^{-1} $MnSO_4$ + 1.0 mol·L^{-1} $(NH_4)_2SO_4$ + Zn^{2+} or PAM at various concentrations at a scan rate of 5 mV·s^{-1} between -1.65 V and -0.8 V, respectively, the concentration of SO_2 was 0.2 g·L^{-1} and pH was 7.4 . As

shown in Fig. 2a, there was no obvious change showed for the cathodic peak current at -1.45 V by adding 0.5 mg·L^{-1} Zn^{2+} to solution 0.455 mol·L^{-1} $MnSO_4$ + 1.0 mol·L^{-1} $(NH_4)_2SO_4$. When the Zn^{2+} concentration increased to 2 mg·L^{-1}, however, the peak current decreased apparently, suggesting that the hydrogen reduction process was slowed. Further observed the ending current at -1.65V after adding Zn^{2+}, the general trends decreased. Furthermore, with the increasing of the Zn^{2+} concentration, the anodic peak current increased accordingly. It was found that the ratio of Qa / Qc increased from 0.040 to 0.054, increasing 35%, while the higher ratio of Qa / Qc was corresponding to a higher deposition efficiency of manganese.

Fig. 2b showed the polarization curves of manganese deposition with various concentration of PAM in solution 0.455 mol·L^{-1} $MnSO_4$ + 1.0 mol·L^{-1} $(NH_4)_2SO_4$. It was found that the peak current of hydrogen evolution reaction did not get obvious changed in the presence of PAM, which means PAM has no obvious effect on evolution of hydrogen reaction. By further negatively polarizing to -1.65V, the corresponding ending current slightly decreased with the addition of PAM from 0 to10 mg·L^{-1}, while the anodic peak significantly increased with the increasing of the PAM concentration by switching the potential scan to the anodic direction. We suspect that the deposited manganese become more dense and compact with the addition of PAM, which could be verified by SEM in later discussion.

To further distinguish the effects of Zn^{2+} and PAM on hydrogen evolution reaction, the cyclic voltammetry measurements were carried out on the same electrode in 1.455 M $(NH_4)_2SO_4$ (free of Mn^{2+}) at a scan rate of 5 mV·s^{-1} by adding 2.0 mg·L^{-1} Zn^{2+} and 10.0 mg·L^{-1} PAM, respectively. As shown in Fig. 3, a current peak was observed at -1.47 V vs. SCE, with the addition of Zn^{2+}, which can be attributed to the reduction of Zn [28]. The cathodic current decreased when further negatively polarized. Apparently, the reduction of zinc plays an important role in promoting cathodic efficiency due to the fact that the overvoltage of hydrogen evolution reaction on zinc is higher than that on manganese or stainless steel. As for the CV with the addition of PAM, it was almost the same as that in blank, which indicates that PAM has no effect on the cathodic current. Moreover, this result verified the effects of PAM on the manganese electrodeposition.

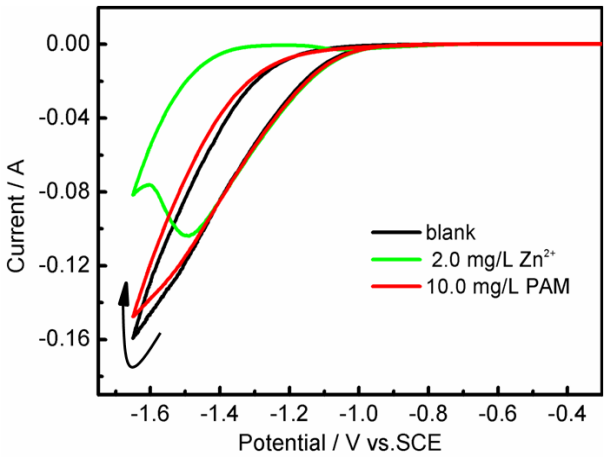

Figure 3. The cyclic voltammograms obtained on a 316 L stainless steel electrode in 1.455 mol·L^{-1} $(NH_4)_2SO_4$ from -1.65 V to -0.3 V at a scan rate of 5 mV·s^{-1}, concentration of SO_2 was 0.2 g·L^{-1}, pH 7.4

3.2. Effect of Zn^{2+} or PAM on current efficiency

Since Zn^{2+} and PAM showed different functions for manganese deposition, it was necessary to compare the current efficiency quantitatively in the same electrolytes S_0 and S_0 + Zn^{2+} or PAM at various concentrations. In order to obtain good coverage, the electrolytic time was set at 2.5 h, the temperature was set at 40 °C, and the current density was set at 50 $mA \cdot cm^{-2}$. The results are listed in Table1.

Table 1. Effect of Zn^{2+} or PAM at various concentrations in solution 0.455 $mol \cdot L^{-1}$ $MnSO_4 \cdot H_2O$ + 1.0 $mol \cdot L^{-1}$ $(NH_4)_2SO_4$, concentration of SO_2 was 0.2 $g \cdot L^{-1}$, pH 7.4

Additive (concentration ($mg \cdot L^{-1}$))	Current efficiency (%)
Zn^{2+} (0)	68.74
Zn^{2+}(0.5)	69.37
Zn^{2+}(1.0)	69.98
Zn^{2+}(2.0)	70.23
PAM(3.0)	68.56
PAM(5.0)	68.42
PAM(10.0)	67.37
Zn^{2+}(1.0) + PAM(5.0)	68.98

The cathodic current efficiency of the manganese electrodeposition in the absence of Zn^{2+} was 68.74%. By adding 1.0 $mg \cdot L^{-1}$ Zn^{2+}, the current efficiency increased by 1% (69.98%), while the increasing of the current efficiency reached to the maximum value of 70.23% by increasing the concentration of Zn^{2+} to 2.0 $mg \cdot L^{-1}$. As for PAM, it was observed that the current efficiency decreased as the PAM concentration increased, and the lowest current efficiency was obtained when the concentration of PAM was 10.0 $mg \cdot L^{-1}$. However, the current efficiency could reach up to 68.98% when a combination of 1.0 $mg \cdot L^{-1}$ Zn^{2+} and 5.0 $mg \cdot L^{-1}$ PAM was added to the solution S_0, which was higher than that of the blank.

3.3. Effect of Zn^{2+} or PAM at various concentrations on optical morphology of the deposited metal

Fig. 4 showed the optical images of the electrolytic manganese metal in the presence and absence of Zn^{2+} in 0.455 $mol \cdot L^{-1}$ $MnSO_4$ + 1.0 $mol \cdot L^{-1}$ $(NH_4)_2SO_4$. Metallic manganese obtained from the Zn^{2+}-free solution was bright. The incorporation of Zn^{2+}, however, did not significantly change the surface appearance.

Fig. 5 showed optical images of the electrolytic manganese metal obtained in absence and presence of PAM. It had been found that by the addition of PAM in aqueous manganese sulfate bath, the metal deposited at the cathode was altered from coarse and granular to soft, compact, and fine. Moreover, the surface of the cathode became smoother. Fabian [29] also found PAM has a significant effect on reducing surface roughness in the electrodeposited copper.

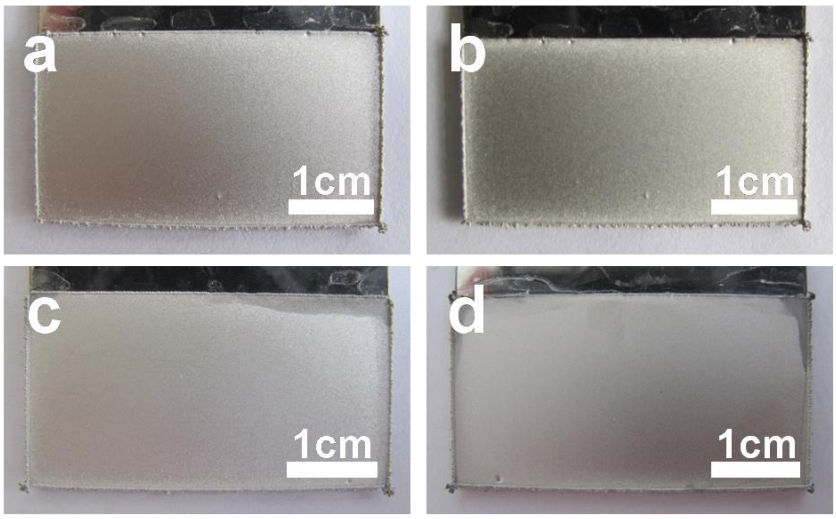

Figure 4. Optical images of electrolytic manganese metal in the presence and absence of Zn^{2+} in 0.455 mol·L^{-1} $MnSO_4$ + 1.0 mol·L^{-1} $(NH_4)_2SO_4$ after 2.5 h of electrolysis. (a) blank, (b) 0.5 mg·L^{-1}, (c) 1.0 mg·L^{-1} and (d) 2.0 mg·L^{-1}, concentration of SO_2 was 0.2 g·L^{-1}, pH 7.4 .

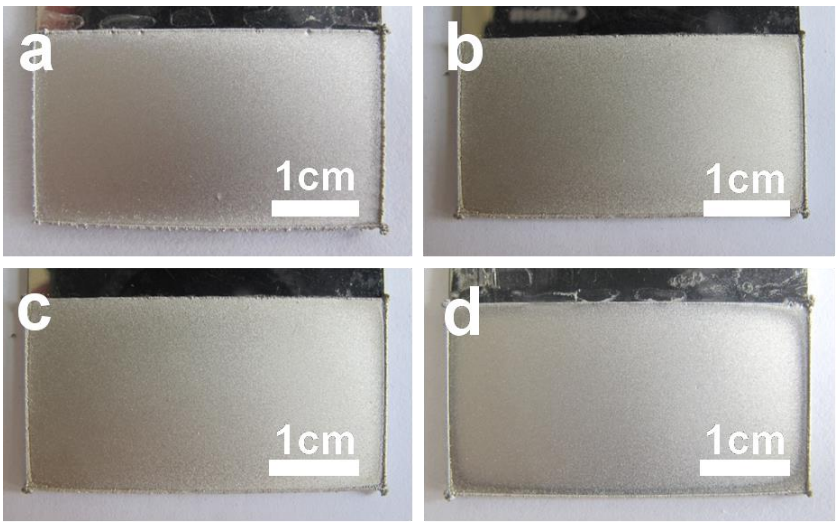

Figure 5. Optical images of electrolytic manganese metal in the absence and presence of PAM in 0.455 mol·L^{-1} $MnSO_4$ + 1.0 mol·L^{-1} $(NH_4)_2SO_4$ after 2.5 h of electrolysis. (a) blank, (b) 3 mg·L^{-1}, (c) 5 mg·L^{-1} and (d) 10 mg·L^{-1}, concentration of SO_2 was 0.2 g·L^{-1}, pH 7.4 .

3.4 The surface morphology of the electrodeposited manganese with or without Zn^{2+} and PAM

To further demonstrate deposition growth of manganese in the absence and presence of Zn^{2+} and PAM, a series of SEM images of the deposit obtained at various electrolysis times under the working conditions were shown in Fig. 6. At the initial stage (1 min), although the size of the metallic manganese particle with the addition of 2 mg·L^{-1} of Zn^{2+} was smaller than that without Zn^{2+} (Fig. 6a), the particle was more compact and smooth (Fig. 6d). With the electrolytic time of 10 min, the average size of the grains was lager in the presence of 2 mg·L^{-1}, which could reach to 2 μm (Fig. 6e). After 150

min of electrolysis, the granular size could reach up to 20 μm. It was worth noting that smaller manganese crystals were found in the presence of Zn^{2+} (Fig. 6f), while the larger granular was found to equally distribute on the cathode, which was free of Zn^{2+}.

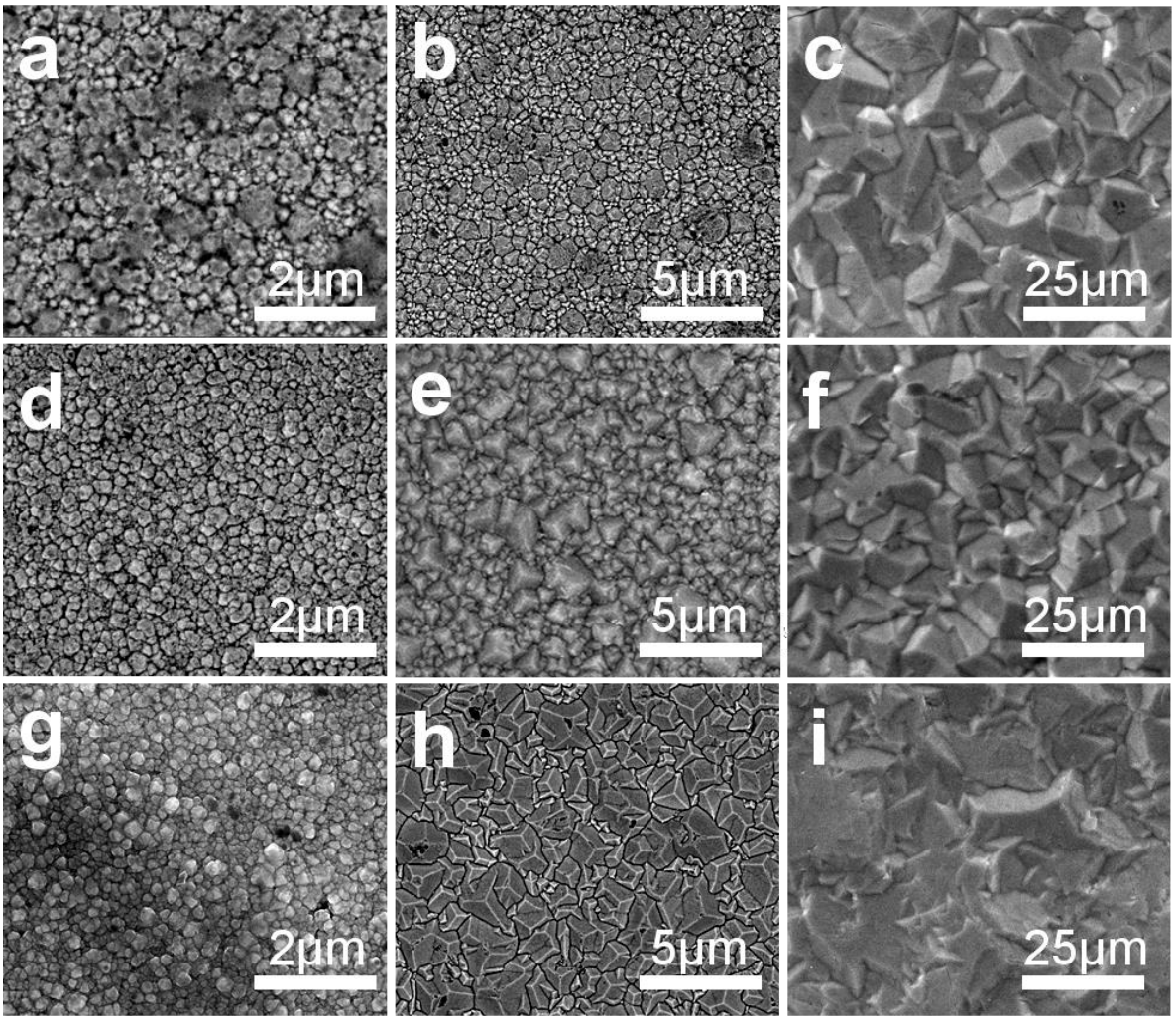

Figure 6. SEM images of electrolytic manganese metal in working solution S_0 with various concentrations of additives for different electrolysis time. (a) S_0, 1 min, (b) S_0, 10 min, (c) S_0, 150 min,(d) S_0 + 2mg·L^{-1} Zn^{2+}, 1 min, (e) S_0 + 2 mg·L^{-1} Zn^{2+}, 10 min, (f) S_0 + 2 mg·L^{-1} Zn^{2+}, 150 min, (g) S_0 + 5 mg·L^{-1} PAM, 1 min, (h) S_0 + 5 mg·L^{-1} PAM, 10 min, (i) S_0 + 5 mg·L^{-1} PAM, 150 min.

This may be attributed to the reduction of Zn^{2+} to Zn, which inhibits the hydrogen evolution reaction and thus accelerates the growth of manganese nucleation, resulting in larger grains during the initial stage (10min). More manganese nucleation was newly initialized when particle reached a certain size, finally, the gaps between larger particles were filled with little grains to produce more compact accumulation associated with high current efficiency of 70.2%.

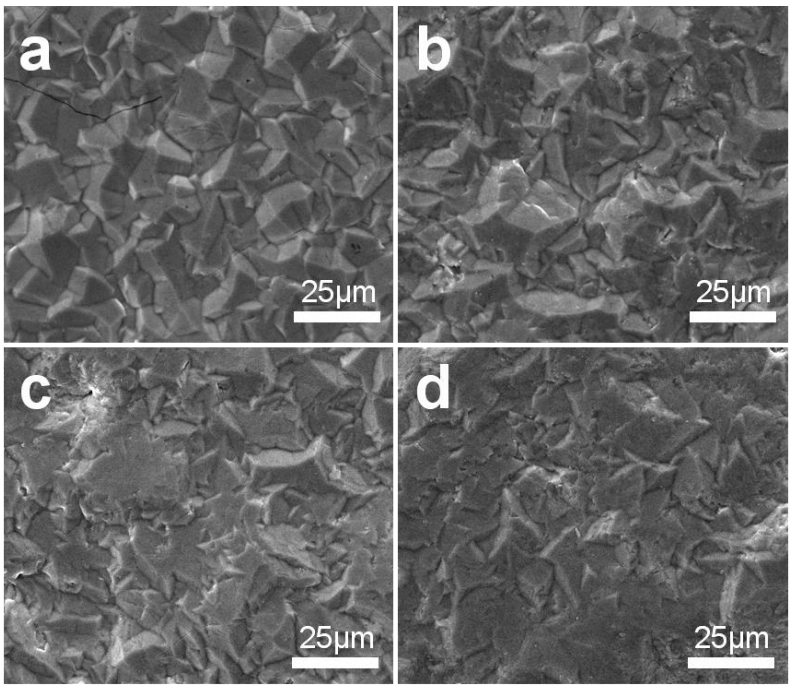

Figure 7. SEM images of electrolytic manganese metal at different concentration of PAM in working solution 0.455 mol·L^{-1} $MnSO_4$ + 1.0 mol·L^{-1} $(NH_4)_2SO_4$ after 2.5 h of electrolysis. (a) blank, (b) 3.0 mg·L^{-1}, (c) 5.0 mg·L^{-1} and (d) 10.0 mg·L^{-1}, concentration of SO_2 was 0.2 g·L^{-1}, pH 7.4 .

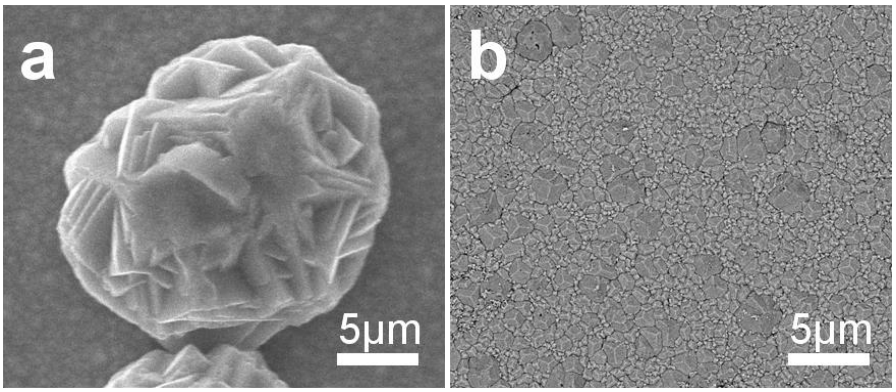

Figure 8. SEM images of electrolytic manganese metal in working solution S_0 with various concentrations of PAM on the edge area of the cathode after 10 min of electrolysis. (a) S_0, (b) S_0 + 5 mg·L^{-1} PAM.

By incorporation of 5 mg·L^{-1} PAM into the electrolyte at the initial deposit for 1min, the grains were more dense and compact (Fig. 6g), indicating that adding PAM to solution S_0 had significant influence on the random crystal orientation, which was in agreement with the result of Li [30]. Due to its particular molecular structure, PAM tends to be absorbed on the surface of the cathode, especially the synergistic adsorption of its polymer chain and amine group and this is beneficial for nuclei formation, thereby leading to a smaller size [31]. Thus, after 2.5h of electrolysis, as shown in Fig. 6h, striking changes were observed on the surface of the deposited metal. The original manganese grain structure could hardly observed due to a large number of fine grains accumulating together to refine

the granular sharp corner, moreover, it should be mentioned that, upon increasing the concentration of PAM, the deposited metal was denser, harder and more compact. SEM images with various concentrations of PAM were presented in Fig. 7, which clearly showed that PAM played an important role on leveling and refinement once the PAM concentration increased to 5mg·L^{-1}. This smooth and compact deposited manganese is hard to dissolve, so the corresponding anodic peak increased significantly (Fig. 2b).

Particularly, remarkable changes had taken place on the edge area of the cathode when 5mg·L^{-1} PAM was incorporated into the electrolyte, as shown in Fig. 8. Generally speaking, due to the uneven current distribution on the cathode plate, the size of grains at the edge of the cathode was larger than those growing at the center of the cathode. However, no extraordinarily large manganese crystal was found at the edge of the cathode plate (Fig. 8b), which should be attributed to the intensely leveling effect of PAM [32]. The unique surface morphology of manganese deposit with the incorporation of PAM is a key feature which can be used for the long-time industrial production.

3.5. XRD analysis of the deposited metal

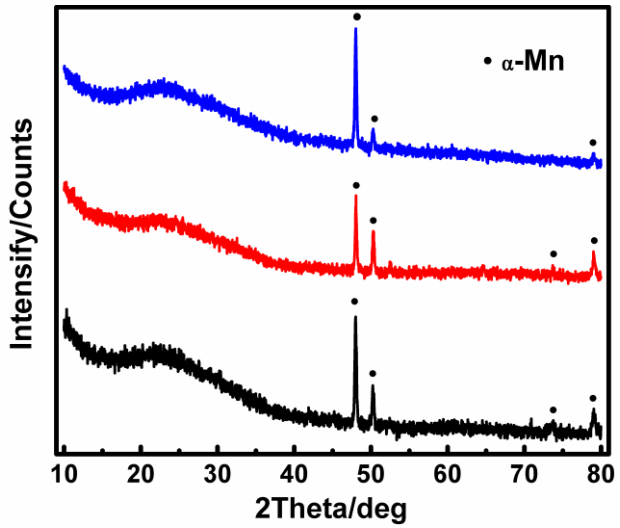

Figure 9. X-ray diffraction patterns of deposited manganese from working solution (S_0) with different additives: black line, S_0; red line, S_0 + 2.0 mg·L^{-1} Zn^{2+}; blue line, S_0 + 10 mg·L^{-1} PAM.

The XRD results (Fig. 9) showed that the coating obtained in the presence of 2 mg·L^{-1} Zn^{2+} and 10 mg·L^{-1} PAM did not change the structure of deposited manganese, which consisted only one phase, namely hard and brittle α-Mn.

3.6. The combination of Zn^{2+} and PAM

Neither C or O element was detected in the deposit (Table 2), indicating PAM was not incorporated into the deposited metal. Hence, the incorporation of PAM did not affect the purity of the deposited metal.

Taking the current efficiency and surface morphology of the deposit into consideration, since no additional beneficial effect was observed by going beyond 5 $mg \cdot L^{-1}$, this value was chosen as the optimal PAM concentration. In view of the mechanism of Zn^{2+} in manganese deposition, and the purity of the deposit, so the complex additive was prepared using these two compounds, and the purity of manganese was measured to make sure whether this combination meets the demand of the production.

Table 2. XRF analysis of the deposited metallic manganese from 0.455 $mol \cdot L^{-1}$ $MnSO_4$ + 1.0 $mol \cdot L^{-1}$ $(NH_4)_2SO_4$ in the presence of 1.0 $mg \cdot L^{-1}$ Zn^{2+} and 5.0 $mg \cdot L^{-1}$ PAM obtained after electrolysis at 50 $mA \cdot cm^{-2}$ for 2.5 h, concentration of SO_2 was 0.2 $g \cdot L^{-1}$, pH 7.4 .

Element	Concentration (%)
Mn	99.90
S	0.033
Zn	0.011
Si	0.052

The results showed that the purity of this deposited metallic manganese was more than 99.90% from working solution (S_0) in the presence of 1.0 $mg \cdot L^{-1}$ Zn^{2+} and 5 $mg \cdot L^{-1}$ PAM obtained after electrolysis at 50 $mA \cdot cm^{-2}$ for 2.5 h, and the current efficiency was 68.98%. Furthermore, when Zn^{2+} and PAM were used, they acted synergistically to increase the current efficiency.

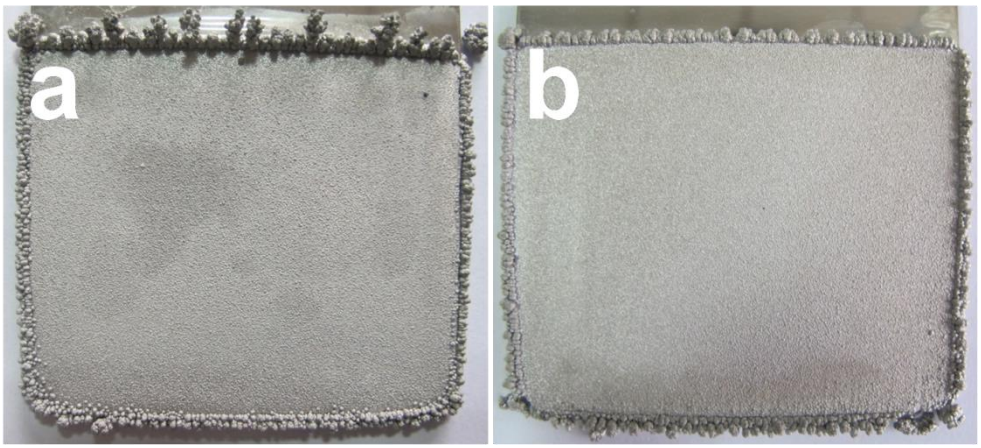

Figure 10. Optical images of electrolytic manganese metal in working solution (a) S_0 and (b) S_0 + 1.0 $mg \cdot L^{-1}$ Zn^{2+} + 5.0 $mg \cdot L^{-1}$ PAM for 24 h of electrolysis.

In addition, the synergistic effect of these two additives was more pronounced after 24 h of electrolysis (Fig. 10). Light, compact and less dendritic deposit was obtained in the presence of these two kinds of additives. This combination of Zn^{2+} and PAM could provide a wide range of possibilities for further development of large-scale applications of manganese.

4. CONCLUSION

The effects of the additives of Zn^{2+} and PAM on the electrodeposition of manganese from non-selenium sulfate solutions have been analyzed through cyclic voltammetry. The results show that Zn^{2+} is preferentially reduced to Zn, which plays an important role in increasing current efficiency by inhibiting the hydrogen evolution reaction, but does not change the surface morphology of the manganese deposit, and it is still an octahedral structure. The incorporation of PAM decreases the current efficiency lightly, but the surface morphology of deposit is apparently leveled because PAM can be adsorbed on the surface of the electrode to improve nucleation formation, then to produce a large number of fine particles to accumulate compactly. The combination of Zn^{2+} and PAM could maintain the current efficiency at a high level (68.98%) and inhibit the growth of dendrite effectively after 24 h of electrolysis. This work has posed a novel way for long time electrodeposited manganese and deepened understanding of additives for the electrodeposition.

ACKNOWLEDGEMENT
This study is financially supported by the Key Project in the National Science & Technology Pillar Program during the Twelfth Five-year Plan Period (2015BAB01B01) and National Natural Science Foundation of China (51325102).

References

1. Z.Z. Tan, G.G. Mei, W.J. Li, K.X. Zeng, N.T. Liang, X.B. Zeng, *Metall. Manganese.* (2004)
2. S.C. Lai, *US Patent.* No. 3821096. (1974)
3. J.E. Lewis, P.H. Scaife, D.A. Swinkels, *J. Appl. Electrochem*. 6 (1976) 453.
4. P. Radhakrishnamurthy, A.K.N. Reddy, *J. Appl. Electrochem.* 7 (1977) 113.
5. P. Ilea, I. Popescu, M. Urdă, L. Oniciu, *Hydrometallurgy*. 46 (1997) 149.
6. S.K. Padhy, P. Patnaik, B.C. Tripathy, I.N. Bhattacharya, *Mater. Sci. Eng. B.* 193 (2015) 83.
7. S.K. Padhy, P. Patnaik, B.C. Tripathy, M.K. Ghosh, I.N. Bhattacharya, *Hydrometallurgy*. 165 (2016) 73.
8. X. Fan, S.Y. Xi, D.G. Sun, Z.H. Liu, J. Du, C.Y. Tao, *Hydrometallurgy.* 127 (2012) 24.
9. P.P. Jiao, F.Y. Xu, J.H. Li, N. Duan, G.Y. Chen, L.H. Jiang, *Int. J. Hydrog. Energy*. 41 (2016) 784.
10. Y. Sun, X.K. Tian, B.B. He, C. Yang, Z.B. Pi, Y.X. Wang, S.X. Zhang, *Electrochim. Acta*. 56 (2011) 8305.
11. J. Lu, D. Dreisinger, T. Glück, *Hydrometallurgy*. 141 (2014) 105.
12. E. Griškonis, A. Šulčius, N. Žmuidzinavičienė, *J. Appl. Electrochem*. 44 (2014) 1117.
13. M. Vinceti, E.T. Wei, C. Malagoli, M. Bergomi, G. Vivoli, *Rev. Environ. Health*. 16 (2001) 233.
14. E. Philip, *Environ. Health. Perspectives*. 86 (1990) 291.
15. J.H. Jacobs, P.E. Churchward, *J. Electrochem. Soc*. 94 (1948) 108.
16. J. Araujo, M. Castro, V. Lins, *Hydrometallurgy*. 84 (2006) 204.
17. P. Wei, O.E. Hileman, M.R. Bateni, X.H. Deng, A. Petric, *Surf. Coat. Technol*. 201 (2007) 7739.
18. C.L. Mantell, G.R. Ferment, *US Patent.* No. US3455799. (1969)
19. W. Zhang, C.Y. Cheng, *Hydrometallurgy*. 89 (2007) 137.
20. A. Sulcius, E. Griskonis, K. Kantminiene, N. Zmuidzinaviciene, *Hydrometallurgy.* 137 (2013) 33.
21. J.H. Jacobs, *US Patent.* No. 3034973. (1962)
22. J.B. Goddard, *US Patent*. No. 4149944. (1979)
23. T.W. Coleman, R.A. Griffin, *US Patent.* No. 4478697. (1984)

24. L. Ding, X. Fan, J. Du, Z. Liu, C.Y. Tao, *Int. J. Miner. Process.* 130 (2014) 34.
25. Q.F. Wei, X.L. Ren, J. Du, S.J. Wei, S.R. Hu, *Miner. Eng*. 23 (2010) 578.
26. M.C. Carosella, R.M. Fowler, *J. Electrochem. Soc*. 104 (1957) 352.
27. J. Gong, G. Zangari, *J. Electrochem. Soc.* 149 (2002) 209.
28. D. Sylla, C. Savall, M. Gadouleau, C. Rebere, J. Creus, P. Refait, *Surf. Coat. Technol*. 200 (2005) 2137.
29. C. Fabian, M.J. Ridd, M. E. Sheehan, *Hydrometallurgy*. 84 (2006) 256.
30. M.C. Li, L.L. Jiang, W.Q. Zhang, Y.H. Qian, S.Z. Luo, J.N. Shen, *J. Solid. State. Electrochem*. 11 (2007) 549.
31. Q.Y. Li, W. Ge, P.X. Yang, J.Q. Zhang, M.Z. An, *J. Electrochem. Soc*. 163 (2016) 127.
32. C. Fabian, M.J. Ridd, M. E. Sheehan, *Hydrometallurgy*. 86 (2007) 44.